An Effective Rewriting of the Inverse Scattering Equations via Green's Function Decomposition

Martina T. Bevacqua and Tommaso Isernia

Abstract—In this paper, a new inversion model for two-dimensional microwave imaging is introduced by means of a convenient rewriting of the usual Lippmann–Schwinger integral scattering equation. Such model is derived by decomposing the Green's function and the corresponding internal radiation operator in two different contributions, one of them easily computed from the collected scattered data. In case of lossless backgrounds, the resulting model turns out to be more convenient than the traditional one, as it exhibits a lower degree of non-linearity with respect to parameters embedding the unknown dielectric characteristics. This interesting property suggests its exploitation in the solution of the inverse scattering problem. The achievable performance is tested by comparing the proposed model with the usual one based on the usual Lippman-Schwinger equation in both cases of linearly approximated and full non-linear frameworks. Both numerical and experimental data are considered.

Index Terms—Born approximation; Contrast Source Inversion; Green's function; inverse scattering; microwave imaging; non-linearity; radiating currents.

I. INTRODUCTION

THE development of effective and accurate techniques for the solution of inverse scattering problems [1]-[2] plays a pivotal role in very many as well as relevant microwave applications, such as biomedical imaging, subsurface prospecting and non-destructive testing [3]-[6]. The adopted mathematical models for describing the electromagnetic scattering phenomena significantly affect the reliability and the achievable performance [7]-[9]. As a consequence, a large attention has been paid on the analysis and formulation of new scattering models able to enlarge applicability and accuracy of the adopted inversion techniques. In particular, scattering models are of interest such to reduce as much as possible the non-linearity of inverse scattering problems, and, hence, counteract the false solutions problem [10].

With respect to the two-dimensional geometry and scalar field case, some analyses have been performed to quantify the 'degree of non-linearity' (DNL) of the relationship between the unknown permittivity profile and the scattered field as a measure of the difficulty of inverse scattering problems. In particular, the DNL has been evaluated depending on the scatterer size as well as on the maximum magnitude of the unknown permittivity profile [7]. The larger the permittivity and/or the target dimensions, the higher the non-linearity of inverse scattering problems. The non-linearity of inverse scattering problems can be mathematically explored through the 'state' equation, that is the Lippmann–Schwinger integral equation, which relates the induced current/total field inside the investigation domain to the unknown target properties. As such, the DNL has been proved to be strictly connected to the norm of the radiation operator adopted in the state equation, which takes into account multiple scattering effects [7].

To reduce the non-linearity, in [8] a convenient rewriting of the scattering equations has been derived from the traditional ones by taking advantage from the peaked behavior of the Green's function in lossy media and without adopting any approximation. Such rewriting of the equation modeling the scattering phenomena has allowed a reduction of the DNL of the problem. The approach has been also proved to be useful in case of lossless backgrounds [9].

In the same spirit, in [11] a family of new integral equations has been introduced, which are transformed from the original Lippmann–Schwinger integral equation and wherein the model in [8],[9] can be seen as a specific case. In such models, issues arising from non-linearity are effectively alleviated, and, again, no approximation is involved.

Encouraged from the results in [8],[9],[11], in this paper a new mathematical model is introduced to solve inverse scattering problems in lossless and homogenous background medium which is based on a convenient decomposition of the Green's function and the corresponding internal radiation operator. In fact, one of the two resulting integrals turns out to be easily computable from the scattered field, as preliminary discussed in [12]. Notably, such contribution, by virtue of the results in [13], is indeed related to (a part of) the radiating currents [14],[15] induced inside the unknown target. Such circumstance suggests some connections with the Subspace Optimization Method (SOM) [16] and the SOM-related non-iterative method introduced by X. Chen et al. in [17]. However, some differences amongst SOM and the proposed rewriting of

the scattering equations exist. For instance, the herein proposed model is based on the decomposition of the Green's function appearing in the internal operator and leads to a modification of the kernel of the radiation operator appearing in the state equation. Opposite to the proposed method, SOM is based on the decomposition of the induced currents into the so called 'deterministic' and 'ambiguous' parts and keeps unaltered the kernel of the radiation operator.

A Green's function decomposition is also used in [18], wherein a data-driven linearized approach is derived by assuming as an auxiliary unknown the field which would be scattered from the target under the Born approximation (BA) (for the internal field), which is also very different from what follows.

As discussed in the remainder of the paper, the capability to evaluate one of the two integrals resulting from the Green's function decomposition allows to get an equation which has exactly the same structure as the original Lippman Schwinger equations, but with a different and somehow more convenient integral operator. In fact, the introduced model can be proved to exhibit a lower DNL with respect to parameters embedding dielectric characteristics as compared to the traditional scattering equations. As a consequence, the use of the proposed model implies interesting advantages in term of convergence and accuracy of the corresponding inversion procedures. Such benefits are proved in this paper in both linear and non-linear frameworks. In particular, we introduce a new linear inversion method, able to enlarge the range of validity of the classical BA [19], as well as a modified version of the well-known contrast source inversion (CSI) method [20].

The paper is organized as it follows. In Section II, the traditional equations modeling inverse scattering problems are reported and the concept of degree of non-linearity and its relevance are recalled. Section III introduces the new scattering model herein proposed. Finally, in Sections IV and V some numerical analyses are performed to test the proposed model within linear and non-linear frameworks, respectively. In particular, both simulated and experimental single frequency data are processed. Conclusions follow. Throughout the paper, the case of scalar fields and two-dimensional geometry is considered and a time harmonic factor $exp\{j\omega t\}$ is assumed and dropped.

II. STATEMENT OF THE PROBLEM

A. The classical scattering model

Let us consider one or more unknown dielectric scatterers in the investigated domain D. Let Σ denote their support and $\varepsilon_b(\underline{r})$ and $\varepsilon_x(\underline{r})$ the complex permittivities of the background medium and the unknown targets, respectively, with $\underline{r} = (x, y)$. Let us probe D with some transmitting antennas located at $\underline{r}_t \, \epsilon \, \Gamma$ outside D. The classical model describing the scattering phenomenon for the generic incident direction v corresponding to a $\underline{r}_t$ position is composed by two integral equations, the data

and state equations, that are respectively given by [1]:

$$E_s^v(\underline{r}_m) = \int_D G_b(\underline{r}_m, \underline{r}') \chi(\underline{r}') E_t^v(\underline{r}') dr' = A_e[W^v(\underline{r})]$$

(1)

and

$$\begin{aligned} W^v(\underline{r}) &= \chi(\underline{r}) E_i^v(\underline{r}) \\ &\quad + \chi(\underline{r}) \int_D G_b(\underline{r}, \underline{r}') \chi(\underline{r}') E_t^v(\underline{r}') dr' \\ &= \chi(\underline{r}) E_i^v(\underline{r}) + \chi(\underline{r}) A_i[W^v(\underline{r})] \end{aligned}$$

(2)

where $\chi(\underline{r}) = \frac{\varepsilon_x(\underline{r})}{\varepsilon_b(\underline{r})} - 1$ is the contrast function which encodes the electromagnetic properties of the unknown objects, $E_s^v(\underline{r}_m)$ is the scattered field measured by different receivers located at $\underline{r}_m \, \epsilon \, \Gamma$ outside D. $W^v = \chi E_t^v$, E_t^v and E_i^v are, respectively, the so called contrast sources, the total and incident electric fields in D. A_e and A_i are short notations of the external and internal radiation operators, respectively. Finally, $G_b(\underline{r}, \underline{r}') = -\frac{j}{4} k_b^2 H_0^2(k_b|\underline{r} - \underline{r}'|)$ is the Green's function pertaining to the background medium[1], being H_0^2 the zero order and second kind Hankel function and $k_b = \omega\sqrt{\mu_b \varepsilon_b}$ the wavenumber in the host medium.

The equation (2) is the Lippman Schwinger equation and relates the contrast source/total field inside D to the contrast function χ [1]. For the sake of brevity as well as for emphasizing the differences with the one proposed in the following, let us identify the model (1)-(2) as the H0 model.

B. A measure of the 'degree of non-linearity'

In order to establish the complexity and difficulty of the inverse scattering problem at hand, a key role is played by the norm of the operator $A_i X$ involved in the state equation (2), (wherein $X(\cdot)$ is the diagonal operator that gives the product χ times $(\cdot)$). If the l_2-norm $\|A_i X\|$ is lower than 1, the inverse operator $(I - A_i X)^{-1}$, which relates the total field to the incident one, can be expanded in a Neumann series[2] as follows [7]:

$$(I - A_i X)^{-1} = I + A_i X + (A_i X)^2 + \cdots + (A_i X)^n + \cdots$$

(3)

wherein I is the identity operator. From the above series, one can infer that the overall DNL of a given scattering problem increases with the norm of the operator $A_i X$. In fact, one can foresee what is the minimum number of terms required to achieve a given approximation accuracy [7]-[9]. For example, if $\|A_i X\| \ll 1$, one can just consider the first term and a linear relationship holds true between data and unknowns [19]. On the other hand, by truncating the series at the second term, the scattered field can be expressed as a quadratic function of the

---

[1] The background medium is assumed to be homogeneous and lossless.
[2] $\|A_i X\| < 1$ is a sufficient condition for writing the series (3).

contrast [21]. If $\|A_i X\| < 1$, for every given accuracy, a polynomial relationship holds true between data and unknowns of the inverse problem, and the order of the polynomial depends on how large is $\|A_i X\|$. If $\|A_i X\| > 1$, a non-polynomial relationship instead holds true between data and unknowns. As a consequence of the above, the larger $\|A_i X\|$, the larger the DNL and the overall difficulty of the problem [7]-[9]. In fact, the cost functional, whose global minimum defines the solution of the inverse problem, is a polynomial with a doubled order with respect to the one defined from the series in (3). Hence, the value of $\|A_i X\|$ also gives a quantitative information on the possible number of local minima (corresponding to so called 'false' solutions [10]) of the cost functional at hand.

Then, understanding the factors affecting $\|A_i X\|$ is fundamental in order to keep under control the occurrence of false solutions. In this respect, note that, by applying the Schwarz's inequality, an upper bound to $\|A_i X\|$ can be obtained as:

$$\|A_i X\| < \|X\| \|A_i\|$$

(4)

In such a way, the role played by the integral operator A_i, which only depends on the kernel and on the domain of the integral operator, is separated by the one played by the contrast function χ, which accounts for the properties of the unknown targets. Hence, for a fixed contrast function the non-linearity of the problem depends on the properties of the integral operator appearing in the state equation.

Then, by using (4), a (sufficient) condition for the applicability of the series (3), as well as additional information about its DNL, can be gained by separately investigating $\|X\|$ and $\|A_i\|$.

III. A NEW SCATTERING MODEL FROM GREEN'S FUNCTION DECOMPOSITION

The Green function is the solution of the wave equation for a point source. It is the impulsive response of the system. Indeed, if the Green function is known, the solution of the wave equation due to a general source can be deduced thanks to the linear superposition [22].

According to [23], the Green's function is the superposition of a homogenous and inhomogeneous components. Both of them include propagating waves, while the homogeneous parts contain only propagating ones. Moreover, the singularity of the Green function is contained completely in the inhomogeneous part.

By exploiting the properties of the Hankel function [24], the Green's function in (1)-(2) can be decomposed in two terms, containing respectively the zero order Bessel functions of the first kind J_0 and second kind Y_0, i.e.:

$$G_b(\underline{r}, \underline{r}') = -\frac{jk_b^2}{4} J_0(k_b|\underline{r} - \underline{r}'|) - \frac{k_b^2}{4} Y_0(k_b|\underline{r} - \underline{r}'|)$$

(5)

The first and second terms represent, respectively, the homogenous and inhomogeneous components of the Green's function [23]. The Bessel functions J_0 and Y_0 in the above equation exhibit different properties both in the spatial and spectral domains [24]. For instance, unlike J_0, Y_0 exhibits a singularity in $\underline{r} = \underline{r}'$. Moreover, J_0 has a spectral content only concentrated in the circle of radius k_b. On the other side, the inhomogeneous part of the Green function, that is Y_0, has positive spectral components outside the circle of radius k_b, zero on it and negative inside it [23].

Then, by exploiting the decomposition of the Green's function in homogeneous and inhomogeneous parts, the internal radiation operator A_i can be split into the sum of two new integral internal operators $A_i^{J_0}$ and $A_i^{Y_0}$, i.e.:

$$A_i[W^v] = -j\frac{k_b^2}{4} \int_D J_0(k_b|\underline{r} - \underline{r}'|) W^v(\underline{r}') d\underline{r}'$$
$$- \frac{k_b^2}{4} \int_D Y_0(k_b|\underline{r} - \underline{r}'|) W^v(\underline{r}') d\underline{r}' =$$
$$= A_i^{J_0}[W^v] + A_i^{Y_0}[W^v] = -j\frac{k_b^2}{4} F_{J_0}{}^v + A_i^{Y_0}[W^v]$$

(6)

As discussed in the following subsection, the first integral at the left hand of the equality (6), which in the following is referred as $F_{J_0}{}^v$, can be easily computed from the collected scattered data.

A. On the meaning and computation of $F_{J_0}{}^v$

The first integral in (6) can be seen as the convolution product between the induced contrast sources and the relevant zero order Bessel function J_0. Hence, due to the spectral properties of the Bessel function J_0 [23],[24], the first convolution product in (6) extracts the spectral component of the currents located on the circle of radius k_b [13]. This is a very interesting circumstance as, by virtue of results in [14],[15],[25],[26], radiating sources oscillate indeed at those frequencies (but for subtleties related to the finiteness of sources). As a consequence, the first part of the decomposition in (6) can be related to the radiating currents [13]. In particular, it can be interpreted as the main contribution of the radiating currents (see [13] for more details), i.e. the one lying on the circle of radius k_b in the spectral domain, while the remaining part is still present in the second term $A_i^{Y_0}$ [23],[25]. As a consequence, $F_{J_0}{}^v$ can be understood as the contribution to the total field inside D by the main spectral component of the radiating currents, which are indeed peaked in the spectral domain along the circle of radius k_b [23],[25].

It is important to note that some differences exist with respect to SOM [16]. Indeed, SOM is based on the decomposition of the currents into the so called 'deterministic' and 'ambiguous' parts [16]. In particular, in SOM the CSI method is rewritten by taking into account that the deterministic part of the induced current is uniquely determined from the data equation, while the remaining part is optimized during the minimization of the relevant cost functional [16]. The herein proposed model is

instead based on the decomposition of the Green's function appearing in the internal operator, which allows to extract a part of the radiating currents, that is the ones having a very well-defined spectral content located on the circle $k = k_b$.

The natural question then arises on how one can compute $F_{J_0}{}^v$. A first straightforward possibility to compute $F_{J_0}{}^v$, (which is the one adopted in the following numerical tests), takes advantage from the results in [13],[27]. In fact, by virtue of equations (5) and (9) in [13], in case of far field measurement configuration, the first integral in equation (6) can be easily computed from the data as:

$$\int_D J_0(k_b|\underline{r} - \underline{r}'|) W^v(\underline{r}') d\underline{r}' = \alpha \int_\Gamma E_s{}^\infty(\hat{\underline{r}}_m, v)\, e^{jk_b\underline{r}\cdot\hat{\underline{r}}_m}\, d\hat{\underline{r}}_m$$

(7)

wherein $E_s{}^\infty$ is the far-field pattern, α is a constant and $\hat{\underline{r}}_m$ identifies the direction of $\underline{r}_m$ [13]. The identity (9) simply represents the scalar product over the measurement domain Γ of the measured far-field pattern with the test function $e^{-jkr\cdot\hat{r}_m}$, that is nothing but the Green's function in far-field zone apart from a constant.

In case of near field data, a straightforward procedure is also possible by using the identity (see equations (8) and (16) in [27]):

$$\int_D J_0(k_b|\underline{r} - \underline{r}'|) W^v(\underline{r}')\, d\underline{r}' = \int_\Gamma E_s^v(\underline{r}_m)\, K^{TM}(\underline{r}_m, \underline{r})\, d\underline{r}_m$$

(8)

wherein (see eq. (15) in [27]):

$$K^{TM}(\underline{r}_m, \underline{r}) = \frac{1}{2\pi|\underline{r}_m|} \sum_{n=-\infty}^{+\infty} \frac{J_n(k_b|\underline{r}|)}{H_n^2(k_b|\underline{r}_m|)} e^{jn(\hat{r} - \hat{r}_m)}$$

(9)

n is the order of the Bessel and Hankel functions, while Γ is assumed to be a closed curve of radius $|\underline{r}_m|$, wherein the measurements antennas are supposed to be located. The identity (8) represents the scalar product over the measurement domain Γ of the measured data with the conjugate of K^{TM}. Note that, in evaluating this latter by Eq. (9), only the order n belonging to the interval $[-k_b a, +k_b a]$ can be considered, wherein a denotes the radius of a ball that encloses D [28],[29]. Hence, as long as the measurement probes surround the region under test and are located on a closed curve, $F_{J_0}{}^v$ can be easily computed from the collected scattered data according to (7) or (8).

Finally, in case of aspect limited measurement configurations, $F_{J_0}{}^v$ can be computed by taking into account that the radiating sources W_{rad}^v, that are the part of the sources responsible of scattering phenomenon, can be evaluated from the data by solving the inverse source problem described by the data equation (1). To this end, due to the severe ill-posedness, a regularization technique has to be adopted, such as the Truncated Singular Value Decomposition (TSVD) or the Tikhonov regularization [2]. In applying the desired regularization technique, one could also retrieve the spectral components of the radiating currents not lying on the circle k_b. Then, in order to extract just the spectral component located on the circle, which are of interest in evaluating $F_{J_0}{}^v$, one can use the J_0-filter, that is $A_i^{J_0}[W_{rad}^v]$. In fact, as discussed above, the spectral properties of J_0 are such to filter out the contributions located outside $k = k_b$.

B. The Y0 model

By taking into account the above circumstances, the Lippman-Schwinger scattering equation in (2) can be transformed into:

$$W^v(\underline{r}) = \chi(\underline{r})\hat{E}_i^v(\underline{r}) + \chi(\underline{r})A_i^{Y_0}[W^v]$$

(10)

wherein $\hat{E}_i^v(\underline{r}) = E_i^v(\underline{r}) - j\frac{k_b{}^2}{4}F_{J_0}{}^v(\underline{r})$. Together with (1), the state equation (10) identifies the new model, referred in the remainder of the paper as the Y0 model, wherein the unknowns are again the induced sources W and the contrast function χ. Moreover, the structure of the equation concerning the internal fields is identical to the one of H0 model, but the integral internal operator A_i has now been replaced by $A_i^{Y_0}$ and the incident field E_i^v by a new known 'modified incident' field $\hat{E}_i^v$.

Note that, differently from the CS-EB model, introduced and discussed in [8],[9], the geometrical and electromagnetic properties of the targets are here still encoded in the contrast function $\chi(\underline{r})$. As a consequence, there is no need to adopt further procedures to extract the target features. With respect to SOM, our rewriting of the scattering equations leads instead to the definition of a new model, which could be eventually applied in the framework of different inversion methods. On the other hand, SOM does not propose or solve a new scattering model. Rather, it proposes and realizes a clever inversion of the standard scattering equations relying on a specific CSI procedure aided by the extraction of the 'deterministic' part of the internal currents [16].

As equation (10) has exactly the same structure as the traditional 2D scalar integral equation (2), one can use the same solution strategies usually adopted to solve inverse scattering problems, such as linear approximations or CSI based methods.

C. Comparing Y0 and H0 models

The decomposition of the Green's function has involved the definition of a new integral operator $A_i^{Y_0}$. A comparison between the H0 model (1)-(2) and the herein proposed Y0 model (1)-(10) can be performed in terms of DNL.

By virtue of the inequality (4), one can separately analyze the roles of the contrast profile and of the relevant integral operator. In particular, one can compare the quantities at the right-hand side of (4) and of the corresponding inequality which holds true for the Y0 model, i.e.,

$$\|A_i^{Y_0}X\| < \|X\|\|A_i^{Y_0}\|$$

(11)

As the factor $\|X\|$ is the same in the two inequalities (4) and (11), the DNL of the two formulations can be eventually compared by just evaluating $\|A_i^{Y_0}\|$ and $\|A_i\|$.

To this end, a numerical analysis has been performed by considering that both operators depend only on the size (and shape) of D, whereas the electromagnetic characteristics of the (lossless) background medium can be taken into account by properly scaling the wavelength. Therefore, by following the same reasoning in [9] and by considering a circular domain D of radius R, it is possible to build up a plot of the norm of the two operators as a function of R/λ_b, where λ_b is the wavelength in the background medium.

Figure 1 shows the universal plot of $\|A_i\|$ and $\|A_i^{Y_0}\|$, respectively. As can be seen, both norms are of course monotonically increasing functions of R/λ_b. Interestingly, one can notice that $\|A_i^{Y_0}\|$ is always lower than $\|A_i\|$. As such, for a fixed scattering problem, the new proposed model exhibits a lower DNL and, consequently, a lower number of false solutions.

IV. NUMERICAL ASSESSMENT: LINEAR INVERSION

In order to test the new proposed model, a controlled assessment with both simulated and experimental data has been carried out by performing inversions within both a linear and (full) non-linear frameworks. In this section, a comparison between the results obtained by means of the classical BA within the H0 model and a new linear approximation derived from Y0 model has been performed.

In the standard BA, the inverse scattering problem is linearized by assuming the unknown total field D equal to the incident field. This hypothesis is fully satisfied only in case of weak scatterers, when $\|\chi A_i\| \ll 1$.

In the Y0 model, the incident field has been replaced with an equivalent one, which includes the contribution of a part of the radiating sources $F_{J_0}{}^v$. As such, a new linear approximation for the total field E_t^v can be introduced as follow:

$$E_t^v(\underline{r}) \cong E_i^v(\underline{r}) - j\frac{k_b{}^2}{4}F_{J_0}{}^v(\underline{r})$$

(12)

The above approximation is valid when $\|\chi A_i^{Y_0}\| \ll 1$. As shown in figure 1, $\|A_i^{Y_0}\|$ is always lower than $\|A_i\|$, so that a wider range of applicability of approximation (12) is expected. By substituting this latter in the scattering model, the problem becomes linear, but it is still ill-posed, so that it has to be solved in a regularized sense. In the following examples, the TSVD regularization has been adopted [2].

In summary, the proposed linear inversion method derived from Y0 model, in the following referred as Y0-BA, is composed of three different steps:

- evaluation of $F_{J_0}{}^v$ from the data $E_s^v(\underline{r}_m)$;
- evaluation of the approximated total field $E_t^v(\underline{r})$ by eq. (12);
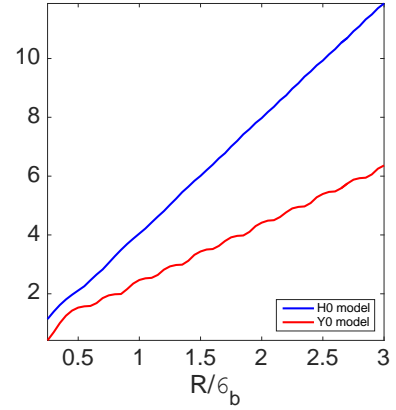- linearization of equation (1) and solution via TSVD regularization.

Figure 1. Universal plot as a function of the electrical size of the region under test: $\|A_i\|$ (blue line) and $\|A_i^{Y_0}\|$ (red line).

It is important to stress that the computation from the data of the term $F_{J_0}{}^v$, which is an additional step with respect to the classical BA, implies a very low computational burden. Indeed, as long as the probes surround the region under test it can be computed by means of the scalar product in (7) or in (8), which is a simple and fast operation. Alternatively, as already noticed in Section III.A, the relevant term $F_{J_0}{}^v$ can be also obtained by preliminary solving the corresponding linear inverse source problem. As such, the computational complexity related to the computation of $F_{J_0}{}^v$ is negligible, and it adds same computational complexity (of the same order as for the original scheme) just in case of measurement probes which do not surround the region under test.

A. Simulated data

In the following numerical analysis two different targets, embedded in free space, have been considered.

Firstly, a homogeneous and lossless kite target has been positioned inside a square domain of side $L = \lambda_b$ and, following [29], 12 receivers and transmitters have been considered, modelled as line sources located on a circumference Γ of radius $R = 10\,\lambda_b$. For more details about the geometry of the kite, the interested readers are referred to Appendix B.

The scattered field data, simulated at the frequency of 300 MHz by means of a full wave forward solver based on the method of moments, have been corrupted with a random Gaussian noise with a SNR = 30dB. Following [30], a number of cells N_c equal to 60×60 has been used in the inversion process, while the direct problems had been solved by considering a double discretization grid.

In order to compare the two models and prove the larger range of applicability of Y0-BA, different values of the contrast function have been considered, in particular, χ=0.3, χ=0.5, χ=0.7 and χ=1. The contrast profiles reconstructed by means of BA and Y0-BA are reported in Figures 2, 3 and 4. In addition, the Figures also depict the profiles corresponding to the ideal case of known total field, that is, the contrast profile estimated
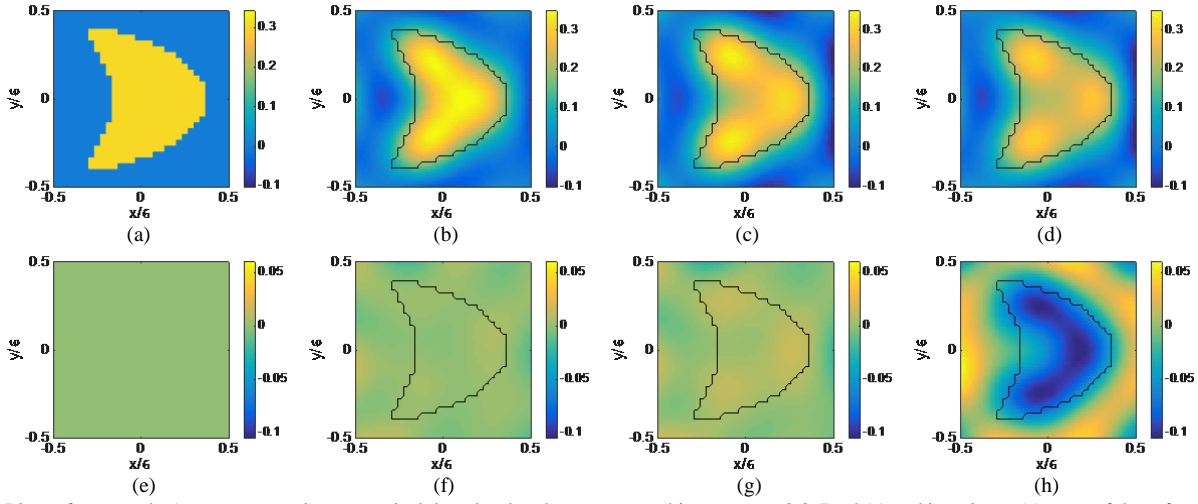
Figure 2. Linear framework. Assessment against numerical data: lossless homogeneous kite target χ=0.3. Real (a) and imaginary (e) parts of the reference profile. Real and imaginary parts of the contrast functions retrieved by assuming known the exact total field (b),(f); by adopting Y0-BA (c),(g) and BA (d),(h).

Figure 3. Linear framework. Assessment against numerical data: lossless homogeneous kite target χ=0.5. Real (a) and imaginary (e) parts of the reference profile. Real and imaginary parts of the contrast functions retrieved by assuming known the exact total field (b),(f); by adopting Y0-BA (c),(g) and BA (d),(h).
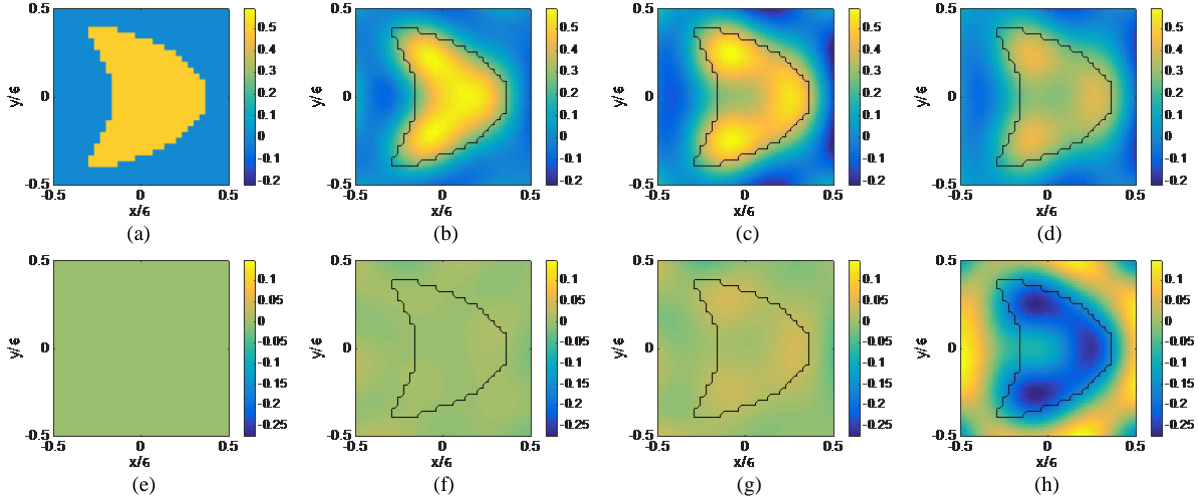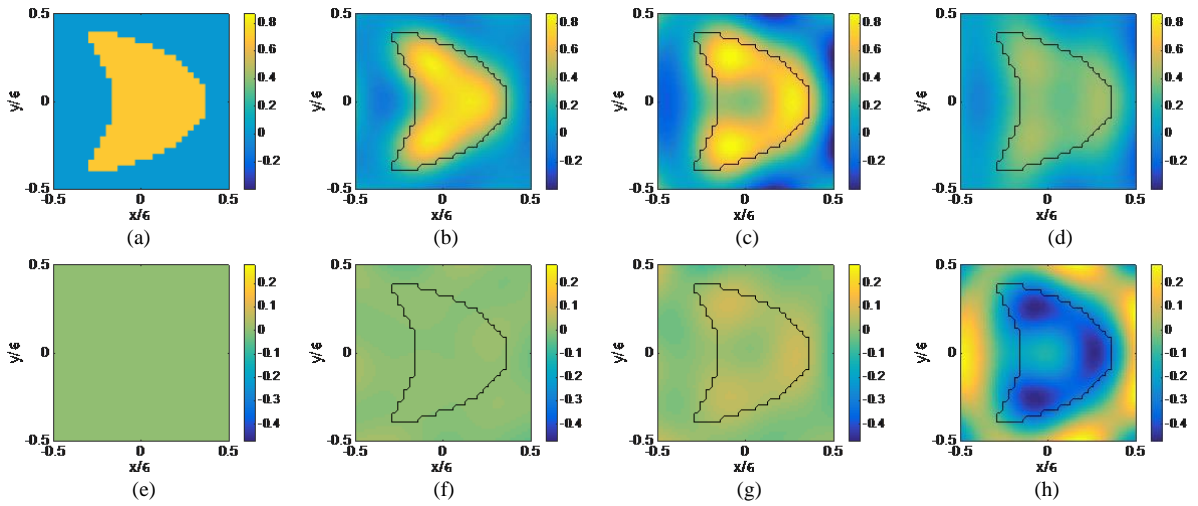

Figure 4. Linear framework. Assessment against numerical data: lossless homogeneous kite target χ=0.7. Real (a) and imaginary (e) parts of the reference profile. Real and imaginary parts of the contrast functions retrieved by assuming known the exact total (b),(f); by adopting Y0-BA (c),(g) and BA (d),(h).

when (1) is inverted by considering the ideal case of knowing the exact total field, rather than the approximated one. While such processing is obviously impossible in practice, it provides a benchmark, being the best possible result that can be achieved from the inversion of the data equation.

In Table I, the normalized mean square errors (NMSE)

between the retrieved contrast function $\tilde{\chi}$ and the actual one χ, defined as:

$$NMSE = \frac{\|\chi - \tilde{\chi}\|^2}{\|\chi\|^2}$$

(13)

are reported in order to quantitatively evaluate the obtained different performance.

Both Figures 2, 3 and 4 and Table I prove that the new proposed model is more convenient than the standard one, as the corresponding linear approximation has a wider range of validity. Indeed, the Y0-BA allows to reach a lower NMSE than BA, and provided χ is not too large, it is also able to exhibit performance similar to the ones obtained in the ideal case.

Then, as second numerical example, the well-known Austria profile with relative permittivity equal to 1.4 has been used as the ground-truth profile. More details about the geometry of the target can be found in Appendix B. The investigation domain of side L = 2.66 λ_b and discretized in $N_c = 64 \times 64$ cells has been investigated by means of 26 receivers and transmitters located on Γ with radius R = 13.3 λ_b. The data have been simulated at the working frequency of 400 MHz by considering $N_c = 128 \times 128$ cells and corrupted with a SNR=30 dB. The results are reported in Figure 5. The mean square errors are, respectively, 0.12 when the total field has been assumed exactly known, 0.41 and and 0.88 when the new linear approximation derived from Y0 model and BA have been adopted, respectively. As can be seen, despite the complexity of the Austria target, Y0-BA retrieves both the electromagnetic properties and shape of the target.

B. Experimental data

In this subsection, the Fresnel targets, typically adopted to benchmark inverse scattering procedures, have been considered, in particular:

- the *TwinDielTM* target [31], consisting of two circular dielectric cylinders with radius 1.5 cm and relative permittivity 3 ± 0.3;
- the *FoamDielIntTM* target [32], which is an inhomogeneous object, constituted by two nested circular cylinders; an outer one made of foam (radius 40 mm, relative permittivity 1.45) that hosts another circular cylinder made of berylon (radius 15 mm and permittivity 3).

The Fresnel data are collected in a partially limited aspect measurements configuration. More details about the targets and the measurement set-up can be found in [31],[32].

For the first target, the investigated area of $0.15 \times 0.15 \, m^2$ has been discretized in 64×64 cells, the working frequency has been selected equal to 4GHz, and a 72×36 multiview-multistatic data matrix has been considered. On the other hand, for the *FoamDielIntTM* target, the investigated area of $0.2 \times 0.2 \, m^2$ has been discretized in 78×78 cells and a 45×36 multiview-multistatic data matrix has been processed

at the working frequency of 3GHz.

The results are reported in Figure 6. As can be seen, BA is not able to quantitatively retrieve the cylinders. As a matter of fact, it can only detect them and retrieve their support. On the other hand, Y0-BA can accurately retrieve both the geometrical and the electromagnetic properties of the considered targets.

	Ideal case	*Y0-BA*	*BA*
χ=0.3	0.13	0.17	0.26
χ=0.5	0.13	0.24	0.44
χ=0.7	0.13	0.3	0.64
χ=1	0.13	0.63	0.96

Table I. Kite target: normalized mean square errors.

V. NUMERICAL ASSESSMENT: NON-LINEAR INVERSION

Encouraged by the interesting results achieved by means of Y0-BA, we have tested the Y0 model within a non-linear regime. In particular, the CSI way of thinking [9],[20] has been adopted to solve the relevant inverse scattering problem.

The CSI method tackles the inverse scattering problem in its full non-linearity, by contemporarily looking for both the contrast χ and the auxiliary unknowns W^v. In particular, the problem's solution is iteratively built by minimizing a cost functional, which takes into account both the misfit in the data and state equations [9].

In the proposed Y0 model, the standard state equation has been substituted by equation (10). Accordingly, from a mathematical point of view, the new CSI method, that in the rest of the paper is referred as Y0-CSI, amounts at retrieving the unknowns of the problem by minimizing the following cost functional:

$$\Phi(W^v, \chi) = \sum_v \frac{\left\| \chi(\underline{r})\hat{E}_i^v(\underline{r}) + \chi(\underline{r})A_i^{Y_0}[W^v] - W^v(\underline{r}) \right\|^2}{\left\| \hat{E}_i^v(\underline{r}) \right\|^2} + \sum_v \frac{\left\| E_s^v(\underline{r}_m) - A_e[W^v] \right\|^2}{\left\| E_s^v(\underline{r}_m) \right\|^2}$$

(13)

Due to the lower DNL of the model, a faster convergence and/or a more accurate solution are expected. In summary, the proposed Y0-CSI involves the following three steps:

- evaluation of $F_{J_0}^{\ v}$ from the data $E_s^v(\underline{r}_m)$;
- redefinition of the internal radiation operator and the incident field;
- minimization of the cost functional in (13) according to some optimization procedure.

As stresses in the previous Section, the first step introduces a

negligible computational complexity. Indeed, the computation of $F_{J_0}{}^v$ is performed outside of the adopted iterative procedure. As far as the second step, a proper discretization of the new scattering equations and in particular of the new internal radiation operator is required. As shown in the Appendix A, as the integrals of the kernel involved in the radiation operator of the Y0 model can be easily computed in a closed form, an FFT based inversion codes can be still used [33]. Consequently, no price is paid in terms of computational complexity when considering the new internal operator.

In this paper, the optimization of the cost functional in (13) is pursued within a conjugate gradient scheme. Moreover, the initial guess is given by the back-propagation solution. More details can be found in [9],[20].

In order to test and assess Y0-CSI, a comparison has been performed with the results obtained by means of standard CSI method, in the following referred as H0-CSI. In case of simulated data, no additional regularization technique has been adopted. On the other hand, in case of experimental data, the cost functional (13) has been equipped with an additive regularization term. In particular, a total variation regularization has been considered by adding a penalty term, which aims at enforcing a piecewise constant target, i.e:

$$\Phi_P(\chi) = \frac{k^2}{2}\left\|\eta(\underline{r})\mathcal{D}_h[\chi(\underline{r})]\right\|^2 + \frac{k^2}{2}\left\|\eta(\underline{r})\mathcal{D}_v[\chi(\underline{r})]\right\|^2 \tag{14}$$

wherein $k = N_c{}^{-1}$, $\mathcal{D}_h$ and $\mathcal{D}_v$ represent the partial derivatives with respect to the horizontal and vertical coordinates of the reference system, respectively. $\eta(\underline{r})$ is a weight function which normalizes $\mathcal{D}_h[\chi]$ at a given iteration with respect to the one evaluated at the previous iteration [34].

Note that the difference in the regularization technique adopted dealing with simulated and experimental data is essentially due to the fact that the latter represents a more challenging case. In fact, the considered Fresnel data are collected in a partially limited aspect measurements configuration [31],[32]. Moreover, as the database provides the incident field only at the receiving locations, the incident fields inside the imaging domain have been estimated from these latter by means of the interpolation procedure outlined in [35], which of course involves some unavoidable model errors.

A. Simulated data

In the following numerical tests, the same targets as the ones in Section IV have been considered.

For the kite target, the following parameters have been considered: a contrast value equal to 1-0.6j, $L = 2\lambda_b$, 20 receivers and transmitters, $R = 2\lambda_b$, a working frequency of 300 MHz, SNR = 20dB and $N_c = 60 \times 60$. As far as the Austria profile, a contrast of 1 has been considered with $L = 2.66\lambda_b$, $N_c = 64 \times 64$, 18 receivers and transmitter, $R = 4\lambda_b$, SNR=20 and a working frequency of 400 MHz. Note that in both cases a doubled grid has been considered in simulating the data.

The results are reported in Figure 7. As far as the kite target is concerned, the NMSE are 0.25 and 0.55 when Y0-CSI and H0-CSI methods have been adopted, respectively. As can be seen, the H0-CSI completely fails in retrieving the permittivity of the target and overestimates the imaginary part. On the other hand, in case of Austria target, the new CSI method allows one to retrieve the properties of the target with a $NMSE = 0.17$. Results obtained by means of H0-CSI are not shown as it completely fails in retrieving the target ($NMSE = 1$).

Besides the advantages in accuracy (which by themselves would be a significant result), the new model also allows a non-negligible reduction of the numbers of iterations. In order to show this remarkable advantage offered by the new model, different values of the contrast functions χ have been considered for the kite target. By observing Table II, one can conclude that a significant amount of iterations is saved, but for the last case wherein the standard model actually fails in retrieving the unknown target, so that its computational burden is not of interest.

B. Experimental data

In this subsection, the *TwinDielTM* target at a working frequency of 6 GHz has been considered. The region of interest of $0.15 \times 0.15\ m^2$ has been discretized in 64×64 cells, and a 18×18 multiview-multistatic data matrix has been processed.

Results, using the Y0-CSI method, are shown in Figure 7(g)-(h). As can be seen, both the shape and electromagnetic properties of the targets are accurately retrieved. On the other hand, the H0-CSI method is not able to retrieve the target. As a consequence, the retrieved profile is not shown.

	$Y0-CSI$		$H0-CSI$	
	NMSE	# iter	NMSE	# iter
χ=1-0.3j	0.18	1453	0.26	1861
χ=1-0.4j	0.20	1388	0.3	1765
χ=1-0.5j	0.22	1383	0.34	1556
χ=1-0.6j	0.25	1276	0.55	549

Table II. Kite target: convergence analysis.

VI. CONCLUSION

The mathematical model adopted for the solution of inverse scattering problems can significantly condition the reliability and achievable performance. In this paper, with reference to 2D scalar problem, a new model for the solution of inverse scattering problem is introduced and tested against both numerical and experimental single frequency data. In particular, the new model, referred as Y0 model, is derived from a convenient decomposition of the Green's function and of the internal radiation operator. Such decomposition has allowed to

rewrite the state equation by extracting a term from the radiation operator which is related to the radiating currents and can be easily computed from the data. The above decomposition has led to a redefinition of the relevant known terms and integral
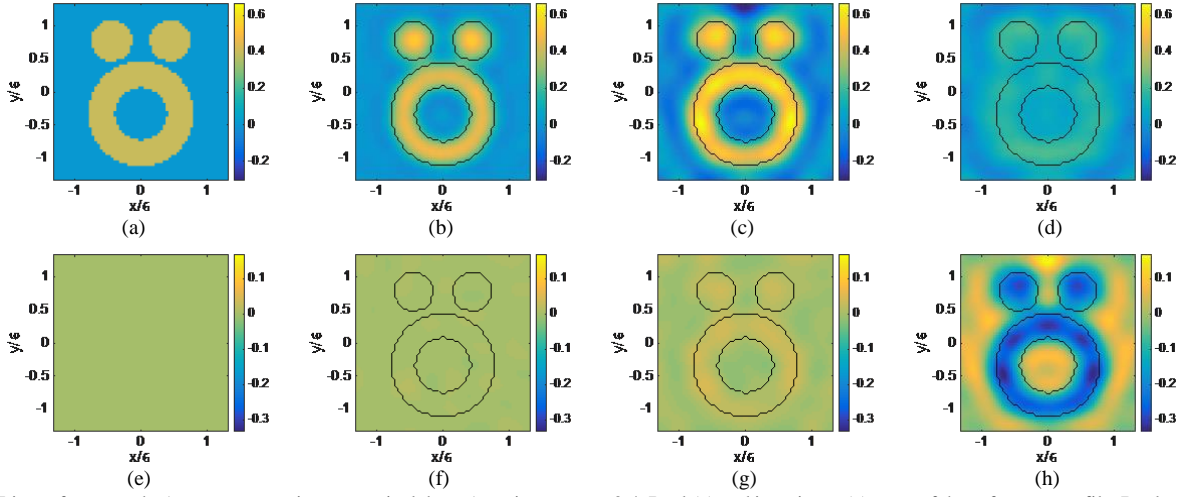
Figure 5. Linear framework. Assessment against numerical data: Austria target χ=0.4. Real (a) and imaginary (e) parts of the reference profile. Real and imaginary parts of the contrast functions retrieved by assuming known the exact total field (b),(f); by adopting Y0-BA (c),(g) and BA (d),(h).
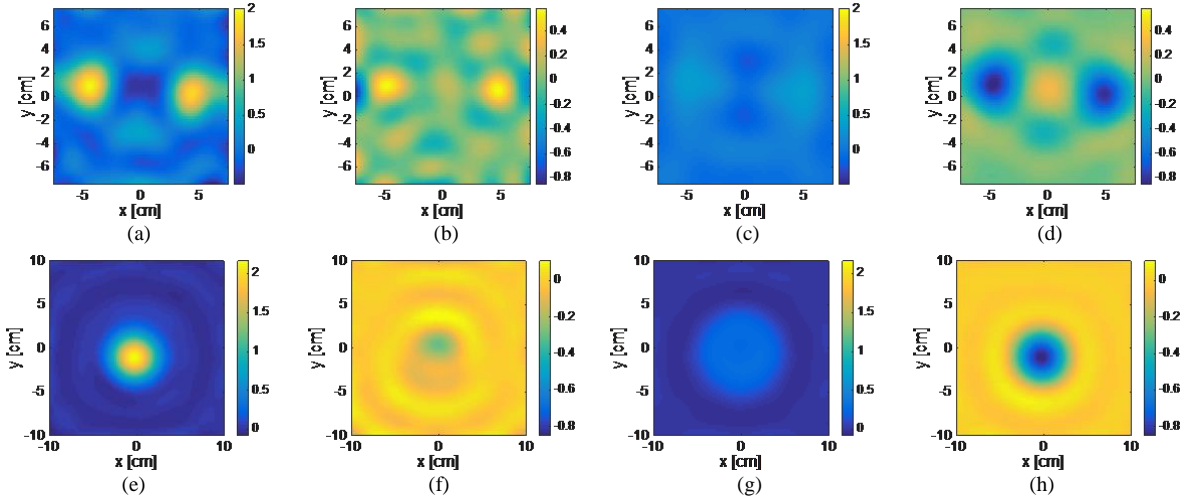

Figure 6. Linear framework. Assessment against experimental data. *TwinDielTM* Fresnel target at 4GHz (a)-(d) and *FoamDielIntTM* Fresnel target at 3GHz (e)-(h). Real and imaginary parts of contrast functions retrieved by adopting Y0-BA (a),(b) and (e),(f), and BA (c),(d) and (g),(h).
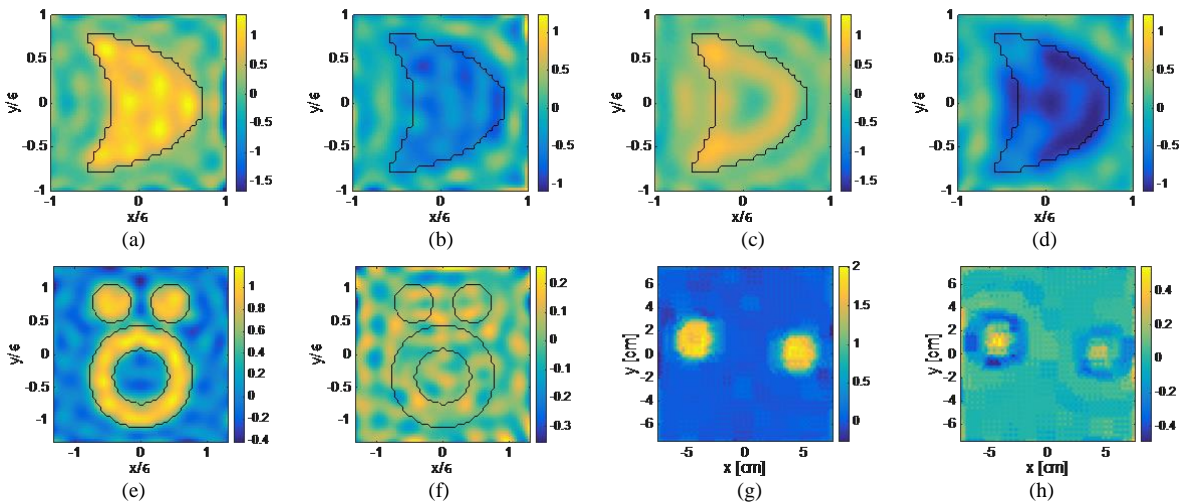

Figure 7. Non-linear framework. Assessment against numerical data (a)-(f): kite target (a)-(d) and Austria target (e)-(f). Assessment against experimental data: *TwinDielTM* Fresnel target at 6 GHz (g)-(h). Real (a),(e),(g) and imaginary (b),(f),(h) parts of contrast function retrieved by adopting Y0-CSI. Real (c) and imaginary (d) parts of the contrast function retrieved by adopting H0-CSI.

operator.

The thus obtained model has been argued to have a lower degree of non-linearity as compared to the classical scattering model by means of a comparison of the norms of the two

relevant integral operators.

Moreover, a new linear approximation of the total field inside the investigation domain has been derived from the new model which definitely outperforms the corresponding linear approximation of the H0 model (i.e., the Born approximation) and exhibit a wider range of applicability. Finally, a modified version of CSI method has been proposed starting from the Y0 model. Due to the lower DNL of the model, faster convergence and more reliable solutions are obtained (without increasing the computational complexity of the inversion scheme), as witnessed by both numerical and experimental data inversions.

Future work will be focused on analyzing actual perspectives of the new model to the more cumbersome case of lossy and/or partially known scenario, as well as to the case of three-dimensional geometries.

APPENDIX A

The proposed rewriting of the scattering equations is based on a different internal operator, which requires a proper discretization. This is a fundamental issue to be addressed for the numerical solution of the inverse problem at hand.

To this end, let us divide the investigation domain into N_c square cells sufficiently small so that the dielectric constant and the electric field intensity are essentially constant over each cell. By paralleling results in the reference paper [30], the new state equation (10) can be rewritten for each view in term of the center of the mth cell:

$$W_m = \chi_m \hat{E}_{i,m} + \chi_m \sum_{n=1}^{N_c} W_n \iint_{cell\ n} -\frac{k_b^2}{4} Y_0(k_b \rho) dx' dy'$$

(A.1)

wherein $W_m, \chi_m, \hat{E}_{i,m}$ represent the contrast source, the contrast function and the electric incident field intensity at the center of the mth cell, $\rho = \sqrt{(x' - x_n)^2 + (y' - y_n)^2}$ and $m=1,2,\ldots,N_c$. As in [30] for the standard model, the above surface integrals can be evaluated in closed form by approximating the square cell with a circular one of radius a. In particular, its expression, referred in the following as $g_{m,n}^i$, becomes:

$$g_{m,n}^i = -\frac{k_b^2}{4} \iint_{cell\ n} Y_0(k_b \rho) dx' dy'$$

$$= \begin{cases} -\frac{\pi a k_b}{2} J_1(k_b a) Y_0(k_b \rho_{mn}) & if\ m \neq n \\ -\frac{1}{2}(\pi a k_b Y_1(k_b a) + 2) & if\ m = n \end{cases}$$

(A.2)

where J_1 and Y_1 are the first order Bessel functions of first and second kind, respectively. Then, the discretized state equation (A.1) can be rewritten as:

$$W_m = \chi_m \hat{E}_{i,m} + \chi_m \sum_{n=1}^{N} W_n\ g_{m,n}^i$$

(A.3)

As $g_{m,n}^i$ is a function of the difference of the Cartesian coordinates of the mth and n^{th} cells, it can be arranged in a 2D sequence and the discretized version of the operator $A_i^{Y_0}$ reduces to a truncated 2-D discrete convolution between the sequence $g_{m,n}^i$, which is as large as twice the dimension of the grid, and the 2-D sequence representing the contrast sources [33].

As a consequence of all the above, also in this case, FFT based inversion codes can be used as in [33], and computational complexity of each iteration of CSI based method keeps unchanged.

APPENDIX B

The kite target is described by the following parametric equation:

$$f(t) = [a \cos t + b \cos 2t - d, c \sin t]$$

(B.1)

where $t \in [0, 2\pi]$, $a = 0.2750, b = 0.1788, c = 0.4125$ and $d = 0.0788$. As far as the kite target in Figure 7, its size is doubled with respect to the one in Figures 2-4.

As far as the Austria target, it consists of an annulus and two disks embedded in the background medium, that is the air. All three scatterers are of same relative permittivity. The two disks are of same radius 0.24 m and their centers locate at (-0.33 m, 0.6m) and (0.33 m, 0.6m). The annulus is centered at (0m, -0.25m) with inner radius of 0.3 m and outer radius of 0.6 m.

REFERENCES

[1] D. Colton and R. Kress, "Inverse Acoustic and Electromagnetic Scattering Theory", *Springer-Verlag,* Berlin, Germany, 1998.

[2] M. Bertero and P. Boccacci, "Introduction to Inverse Problems in Imaging", *Institute of Physics*, Bristol, UK, 1998

[3] M. Pastorino, " Microwave Imaging", *John Wiley*, New York, May 2010.

[4] R. Persico, Introduction to ground penetrating radar: inverse scattering and data processing, *John Wiley & Sons*, 2014.

[5] M. Ambrosanio, M. T. Bevacqua, T. Isernia and V. Pascazio, "The Tomographic Approach to Ground-Penetrating Radar for Underground Exploration and Monitoring: A More User-Friendly and Unconventional Method for Subsurface Investigation," in *IEEE Signal Processing Magazine*, vol. 36, no. 4, pp. 62-73, July 2019.

[6] M. Bevacqua, G. Bellizzi, L. Crocco, T. Isernia, "A Method for Quantitative Imaging of Electrical Properties of Human Tissues from Only Amplitude Electromagnetic Data", *Inverse Problem,* vol. 25, n. 2, 2019.

[7] O. M. Bucci, N. Cardace, L. Crocco, and T. Isernia, "Degree of nonlinearity and a new solution procedure in scalar two-dimensional inverse scattering problems," J. Opt. Soc. Am. A, vol. 18, pp. 1832-1843, 2001.

[8] T. Isernia, L. Crocco and M. D'Urso, "New tools and series for forward and inverse scattering problems in lossy media," *in IEEE Geoscience and Remote Sensing Letters*, vol. 1, no. 4, pp. 327-331, Oct. 2004.

[9] M. D'Urso, T. Isernia and A. F. Morabito, "On the Solution of 2-D Inverse Scattering Problems via Source-Type Integral Equations," in *IEEE Transactions on Geoscience and Remote Sensing*, vol. 48, no. 3, pp. 1186-1198, March 2010.

[10] T. Isernia, V. Pascazio, and R. Pierri. "On the local minima in a tomographic imaging technique", *IEEE Trans. Geosci. Remote Sens.*, vol. 39, pp. 1596-1607, 2001.

[11] Y. Zhong, M. Lambert, D. Lesselier and X. Chen, "A New Integral Equation Method to Solve Highly Nonlinear Inverse Scattering Problems," in *IEEE Transactions on Antennas and Propagation*, vol. 64, no. 5, pp. 1788-1799, May 2016.

[12] M. T. Bevacqua and T. Isernia, "A convenient rewriting to the 2D inverse scattering problem based on the reduced scattered field," *2019 IEEE International Symposium on Antennas and Propagation and USNC-URSI Radio Science Meeting*, Atlanta, GA, USA, pp. 1013-1014, 2019.

[13] M. T. Bevacqua, T. Isernia, R. Palmeri, M. N. Akinci and L. Crocco, "Physical Insight Unveils New Imaging Capabilities of Orthogonality Sampling Method," in *IEEE Transactions on Antennas and Propagation*, vol. 68, no. 5, pp. 4014-4021, May 2020.

[14] A. J. Devaney, and E. Wolf, "Radiating and Nonradiating Classical Current Distributions and the Fields They Generate", *Phys. Rev. D*, vol. 8, no. 4, 1973.

[15] E. A. Marengo and R. W. Ziolkowski, "Nonradiating and minimum energy sources and their fields: generalized source inversion theory and applications," in *IEEE Transactions on Antennas and Propagation*, vol. 48, no. 10, pp. 1553-1562, Oct. 2000.

[16] X. Chen, "Subspace-Based Optimization Method for Solving Inverse-Scattering Problems," in *IEEE Transactions on Geoscience and Remote Sensing*, vol. 48, no. 1, pp. 42-49, Jan. 2010.

[17] T. Yin, Z. Wei and X. Chen, "Non-iterative Methods Based on Singular Value Decomposition for Inverse Scattering Problems," in *IEEE Transactions on Antennas and Propagation*, vol. 68, no. 6, pp. 4764-4773, June 2020.

[18] E. A. Marengo, E. S. Galagarza, and R. Solimene, "Data-driven linearizing approach in inverse scattering," *J. Opt. Soc. Am. A*, vol. 34, pp. 1561-1576, 2017.

[19] A. J. Devaney, "Mathematical Foundations of Imaging, Tomography and Wavefield Inversion", *Cambridge UK: Cambridge University Press*, 2012.

[20] Van den Berg P. M. and Kleinman R. E., "A contrast source inversion method," *Inverse Problem,* vol. 13, pp. 1607–1620, 1997.

[21] A. Brancaccio, V. Pascazio, and R. Pierri, A quadratic model for inverse profiling: the one-dimensional case, in *Journal of Electromagnetic Waves and Applications*, vol. 9, no. 5-6, pp. 673-696, 1995.

[22] W. C. Chew, "Waves and fields in inhomogeneous media". *IEEE press*, 1995.

[23] C. J. Sheppard, S. S. Kou, and J. Lin, "The Green-function transform and wave propagation", *Frontiers in Physics*, vol. 2, no. 67, 2014.

[24] M. Abramowitz and I. A. Stegun, "Handbook of Mathematical Functions with Formulas, Graphs, and Mathematical Tables". NewYork, NY, USA: Dover, 1964.

[25] M. T. Bevacqua and T. Isernia, "On Spectral Content of Radiating Components of Electromagnetic Sources," *2019 International Conference on Electromagnetics in Advanced Applications (ICEAA)*, Granada, Spain, 2019, pp. 0917-0919.

[26] E. A. Marengo and R. W. Ziolkowski, "Non-radiating and minimum energy sources and their fields: generalized source inversion theory and applications," *in IEEE Transactions on Antennas and Propagation*, vol. 48, no. 10, pp. 1553-1562, 2000.

[27] M. N. Akıncı, M. Çayören, and İ. Akduman, "Near-field orthogonality sampling method for microwave imaging: Theory and experimental verification," *in IEEE Transactions on Microwave Theory and Techniques*, vol. 64, no. 8, pp. 2489–2501, 2016.

[28] L. Crocco, L. Di Donato, I. Catapano and T. Isernia, "An Improved Simple Method for Imaging the Shape of Complex Targets," in *IEEE Transactions on Antennas and Propagation*, vol. 61, no. 2, pp. 843-851, Feb. 2013.

[29] O. M. Bucci and T. Isernia, "Electromagnetic inverse scattering: Retrievable nformation and measurement strategies", *Radio Science*, vol. 32, pp. 2123–2138, 1997.

[30] J. Richmond, "Scattering by a dielectric cylinder of arbitrary cross section shape", *IEEE Transactions on Antennas Propag*ation, vol. 13, no. 3, pp. 334-341, 1965.

[31] K. Belkebir and M. Saillard, "Special section: Testing inversion algorithms against experimental data", *Inverse Problem*, vol. 17, pp. 1565–2028, 2001.

[32] K. Belkebir and M. Saillard, "Special section: Testing inversion algorithms against real data: Inhomogeneous targets", *Inverse Problem*, vol, 21, 2005.

[33] T. Isernia, V. Pascazio and R. Pierri, "A nonlinear estimation method in tomographic imaging," in *IEEE Transactions on Geoscience and Remote Sensing*, vol. 35, no. 4, pp. 910-923, 1997.

[34] P. M. van den Berg, A. Abubakar, J. T. and Fokkema, Multiplicative regularization for contrast profile inversion, *Radio Science*, vol. 38, pp. 8022, doi:10.1029/2001RS002555, 2, 2003.

[35] L. Crocco and T. Isernia, 'Inverse scattering with real data: detecting and imaging homogeneous dielectric objects', *Inverse Problem*, vol. 17, no. 6, pp. 1573-1583, 2001.